Spin-torque diode with tunable sensitivity and bandwidth by out-of-plane magnetic field

X. Li,[1] C. Zheng,[1] Y. Zhou,[2,3,a)] H. Kubota,[4] S. Yuasa,[4] and Philip W. T. Pong[1]

[1]*Department of Electrical and Electronic Engineering, The University of Hong Kong, Hong Kong*
[2]*School of Electronics Science and Engineering, Nanjing University, Nanjing 210093, China*
[3]*Department of Physics, The University of Hong Kong, Hong Kong*
[4]*Spintronics Research Center, National Institute of Advanced Industrial Science and Technology, Tsukuba, Ibaraki 305-8568, Japan*

Spin-torque diodes based on nanosized magnetic tunnel junctions are novel microwave detectors with high sensitivity and wide frequency bandwidth. While previous reports mainly focus on improving the sensitivity, the approaches to extend the bandwidth are limited. This work experimentally demonstrates that through optimizing the orientation of the external magnetic field, wide bandwidth can be achieved while maintaining high sensitivity. The mechanism of the frequency- and sensitivity-tuning is investigated through analyzing the dependence of resonant frequency and DC voltage on the magnitude and the tilt angle of hard-plane magnetic field. The frequency dependence is qualitatively explicated by Kittel's ferromagnetic resonance model. The asymmetric resonant frequency at positive and negative magnetic field is verified by the numerical simulation considering the in-plane anisotropy. The DC voltage dependence is interpreted through evaluating the misalignment angle between the magnetization of the free layer and the reference layer. The tunability of the detector performance by the magnetic field angle is evaluated through characterizing the sensitivity and bandwidth under 3D magnetic field. The frequency bandwidth up to 9.8 GHz or maximum sensitivity up to 154 mV/mW (after impedance mismatch correction) can be achieved by tuning the angle of the applied magnetic field. The results show that the bandwidth and sensitivity can be controlled and adjusted through optimizing the orientation of the magnetic field for various applications and requirements. *Published by AIP Publishing.*
[http://dx.doi.org/10.1063/1.4953572]

The spin-transfer torque (STT) of direct current will excite radio-frequency (RF) oscillation in nanosized magnetic tunneling junctions (MTJs), leading to the emergence of spin-torque oscillators.[1] On the other hand, it has also been demonstrated that RF signal can be rectified into DC voltage according to the spin-torque diode effect in MTJ nanopillars,[2] revealing the potential application as microwave detectors.[3,4] When the alternating current (AC) flows through a MTJ nanopillar, the free-layer magnetization oscillates around its equilibrium state, resulting in variable resistance of the device at the AC frequency. The AC is thus mixed with the alternating resistance, leading to a frequency-dependent DC voltage (V_{mix}). Largest DC voltage (V_{DC}) is generated when the ferromagnetic resonant frequency of free layer (f_R) matches that of the applied microwave. The sensitivity of this microwave detector is evaluated as $Sensitivity = V_{DC}/P_{RF}$. The frequency bandwidth is illustrated as the bandwidth of achievable f_R within the available magnetic field range, since f_R can be tuned by the magnitude of magnetic field. The recent report of sensitivity of over 12 000 mV/mW (Ref. 5) and 75 400 mV/mW (Ref. 6) for microwave detection has exceeded that of Schottky diode detectors, showing its great promise for real applications.

In the past decade, efforts have been devoted to increasing the V_{DC} and sensitivity. Previous experimental investigations have revealed that the V_{DC} can be increased by applying a DC bias,[5] by optimizing the in-plane (IP) magnetic field angle,[7] and by adjusting the alignment between the magnetization of the reference layer and the free layer.[8,9] It has also been theoretically predicted that V_{DC} can be optimized by adjusting the orientation of the out-of-plane (OOP) magnetic field.[10] Although several experimental reports show high sensitivity under oblique magnetic field with certain angles,[5,11] there still lacks a systematic experimental investigation of the dependence of V_{DC} on the tilt angle of OOP magnetic field. The bandwidth, on the other hand, is constrained by the available magnetic field range since f_R is primarily determined by the magnitude of external magnetic field (H_{ext}). The introduction of tilt magnetic field offers an additional degree of freedom for extending the frequency bandwidth according to the angular dependence of f_R.[12] Experimental demonstration on how the V_{DC} and f_R can be tuned by the magnitude and tilt angle of OOP magnetic field will be beneficial for improving the performance of spin-torque-diode microwave detectors.

In this work, the spin-torque diode effect in MTJ nanopillar has been investigated under OOP magnetic field. First, the magnetic field is applied in the hard plane, and the dependence of the V_{DC} and f_R on the magnitude and tilt angle is analyzed. Extended bandwidth and increased sensitivity are later demonstrated through tuning the orientation of the magnetic field.

The device under investigation is a $200 \times 100 \, nm^2$ elliptical MTJ nanopillar with a layer structure of Ta 5/CuN 20/Ta 3/

a)Author to whom correspondence should be addressed. Electronic mail: yanzhou@hku.hk

PtMn 15/Co$_{70}$Fe$_{30}$ 2.5/Ru 0.85/Co$_{60}$Fe$_{20}$B$_{20}$ 3/MgO ∼ 1/ Co$_{60}$Fe$_{20}$B$_{20}$ 2/Ta 5/Ru 7 (thickness in nm). When IP magnetic field is applied parallel to the easy axis, the MTJ exhibits parallel resistance-area product of 19 Ω μm^2 and tunnel magnetoresistance (TMR) ratio of 34% (Fig. 1(a)). The experimental setup for spin-torque diode experiment is shown in Fig. 1(b). Microwave power of −30 dBm (1 μW) is pulse-modulated at 8 kHz and injected into the MTJ through a bias-tee. The V_{mix} is measured by a lock-in amplifier when the frequency of microwave current ramps from 2 GHz to 12 GHz. The output power of RF synthesizer is flattened to compensate for the larger loss at higher frequencies. In each measurement, an external magnetic field is applied with polar angle (θ_H) and azimuthal angle (δ_H) (Fig. 1(a) inset) to align the magnetization of free layer (**m**) at (θ_F, δ_F).

First, we explore how V_{DC} and f_R are tuned by the magnitude of hard-plane magnetic field ($\delta_H = 90°$). The magnetoresistance (MR) curves measured at $\theta_H = 0°–90°$ are shown in Fig. 2(a). Under different H_{ext}, the misalignment angle (φ) between **m** and the magnetization of reference layer (**M**) is calculated based on Eq. (1)[5] and shown in Fig. 2(b).

$$R^{-1}(\varphi) = \frac{R_{AP}^{-1} + R_P^{-1}}{2} - \frac{R_{AP}^{-1} - R_P^{-1}}{2} \cos \varphi, \quad (1)$$

where $R(\varphi)$ is the junction resistance, R_{AP} and R_P are the resistances at antiparallel and parallel state, respectively. The anisotropy (H_K) exhibits a shape anisotropy (H_{SA}) at x-axis, an out-of-plane anisotropy (H_{OA}) originated from the MgO/CoFeB/Ta interfaces,[13–15] and a fourfold magnetocrystalline anisotropy (H_{CA})[16] of the partially crystallized CoFeB after annealing.[17] The offset angle (β) between the crystalline easy axis and x-axis results in the asymmetric resistances at negative and positive H_{ext}. When large positive H_{ext} is applied at $\theta_H = 45°$, **m** is rotated to the first octant (1 in Fig. 2(b)), while **M** shifts a small IP angle towards y-axis. This results in a misalignment angle of $\varphi = 50°$. As positive H_{ext} decreases to 0, **m** and **M** gradually resume the initial alignment of $\varphi = 20°$ (2 in Fig. 2(b)). Under increasing negative H_{ext}, **m** is rotated to the seventh octant due to the fourfold H_{CA} (3 in Fig. 2(b)), resulting in the maximum φ of 85°. **m** is aligned back towards the y-z plane when negative $\mu_0 H_{ext}$ is further increased to −0.15 T, leading to decreasing φ towards 60°. It is noted that the resistance and φ change little in the field range of −0.15–0.15 T with $\theta_H = 90°$. This is explained by the small OOP angle of **m** when H_{ext} is much

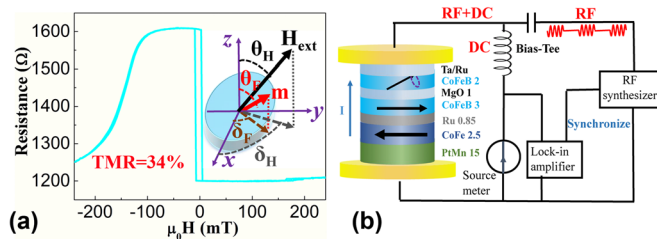smaller than the demagnetization field. In this case, φ is nearly unchanged within the field range.

The changing φ with H_{ext} results in different RF rectification responses. The V_{mix}-frequency spectra measured at $\mu_0 H_{ext}$ ranging from −0.15 T to 0.15 T with $\theta_H = 60°$ are shown in Fig. 2(c). A typical V_{mix}-frequency spectrum is composed of a symmetric Lorentzian peak and an anti-Lorentzian component. The contribution of Lorentzian peak is much larger than the anti-Lorentzian component, indicating the IP component of STT plays a dominant role.[16] The larger φ in negative field results in more IP STT component, so the peaks are higher and more symmetric compared with the peaks at positive field. To evaluate the sensitivity and bandwidth of the detector, the dependences of V_{DC} and f_R on H_{ext} with $\theta_H = 0°–90°$ are shown in Figs. 2(d) and 2(e), respectively. The V_{DC} in a symmetric MTJ can be expressed as[7]

$$V_{DC} = \frac{R_{AP} - R_P}{R_P} \frac{\mu_B}{2e(m_S t A)\sigma} \frac{P}{1+P^2} \frac{R^2}{R_P R_{AP}} \frac{P_{RF}^2}{4} \sin^2 \varphi, \quad (2)$$

where m_S, t, A, and P are the saturation magnetization, thickness, area, and polarization ratio of the free layer, respectively, and σ is the linewidth of the resonant peak. The expression in Eq. (2) is consistent with the experimental results in Fig. 2(d) that V_{DC} reaches maximum at the magnetic field where MR and φ are also largest. The V-shape dependence of f_R on negative H_{ext} with $\theta_H = 0°–90°$ and $\delta_H = 90°$ in Fig. 2(e) can be interpreted qualitatively based on the ferromagnetic resonance model proposed by Kittel[18,19]

$$f_R = \frac{\gamma}{2\pi} \sqrt{H_{effm}(H_{effm} + H_d)} \quad (3)$$

in which $\gamma = 1.76 \times 10^7$ Hz/Oe is the gyromagnetic ratio of electrons, H_d is the demagnetization field, and H_{effm} is the effective field, representing the combined effect of H_{ext} and H_K on **m**. At small H_{ext}, H_K is counteracted by the IP component of H_{ext}, resulting in a reduction in H_{effm} with increasing H_{ext}. So, f_R tends to decrease as H_{ext} increases. The minimum f_R indicates that the free layer is saturated by the IP component of H_{ext}.[20] As H_{ext} further increases, H_{effm} becomes larger and f_R increases accordingly. H_{CA} is responsible for the asymmetric f_R–H_{ext} relation at positive and negative H_{ext}. An analytical model[10,21] is used to quantitatively investigate this f_R–H_{ext} relation with $\theta_H = 45°$ and $\delta_H = 90°$. The magnetic free energy density (F) of the free layer can be expressed as the summation of Zeeman energy (F_{Zeeman}), demagnetization energy (F_{demag}), uniaxial anisotropy energy (F_{UA}), and crystalline anisotropy energy (F_{CA}), defined, respectively, by[21,22]

$$F_{Zeeman} = -m_S H_{ext}[\sin \theta_H \sin \theta_F \cos(\delta_F - \delta_H) \\ + \cos \theta_H \cos \theta_F], \quad (4)$$

$$F_{demag} + F_{UA} = \frac{1}{2} m_S \left[-H_{SA} \sin^2 \theta_F \cos^2 \delta_F \\ + (4\pi m_S - H_{OA}) \cos^2 \theta_F \right], \quad (5)$$

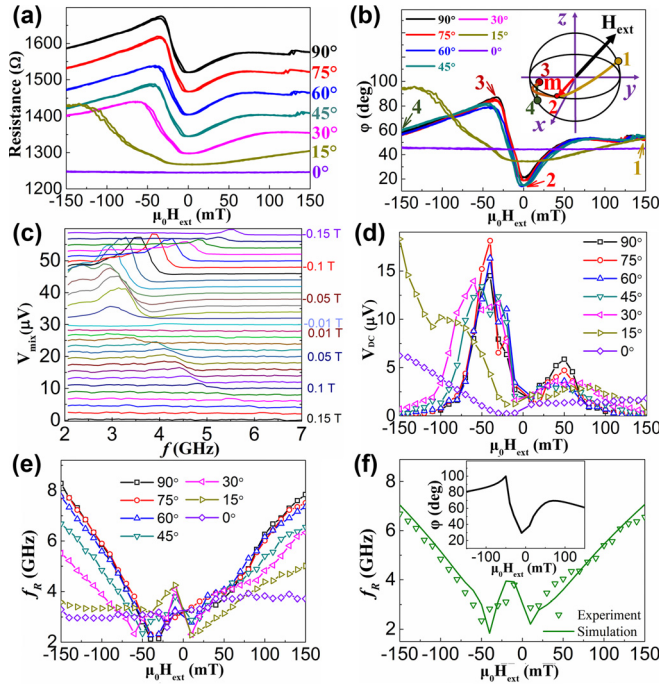$$F_{CA} = \frac{1}{8} m_S H_{CA} \left[\sin^2 2\theta_F + \sin^4 \theta_F \sin^2 2(\delta_F - \beta) \right]. \quad (6)$$

FIG. 1. (a) MR curve measured at $\theta_H = 90°$ and $\delta_H = 0°$ (inset: polar and azimuthal angles of H_{ext} and **m**, where x is the easy axis and z is perpendicular to the film plane). (b) Experimental setup for measuring the spin-torque diode spectrum.

FIG. 2. Influence of magnitude and tilt angle (θ_H) of hard-plane magnetic field. (a) Hard-axis MR curves. (b) φ calculated by Eq. (1) (inset: schematic path of the free-layer magnetization direction when $\mu_0 H_{ext}$ is scanned from 0.15 T to -0.15 T at $\theta_H = 45°$). (c) Spin-torque diode spectrum measured with $\theta_H = 60°$ and $\mu_0 H_{ext}$ from 0.15 to -0.15 T. Each curve is shifted by 2 μV. (d) V_{DC} and (e) f_R measured as a function of H_{ext}. (f) Measured (triangle) and simulated (solid line) f_R-H_{ext} relation with $\theta_H = 45°$ (inset: simulated φ-H_{ext} relation).

The equilibrium angles (θ_F, δ_F) of **m** can be calculated from $\frac{\partial F}{\partial \delta_F} = 0$ and $\frac{\partial F}{\partial \theta_F} = 0$.

$$\frac{\partial F}{\partial \delta_F} = m_S \left[H_{ext} \sin\theta_H \sin\theta_F \sin(\delta_F - \delta_H) \right.$$
$$- \frac{1}{2} H_{SA} \sin 2\delta_F \sin^2\theta_F$$
$$\left. - \frac{1}{4} H_{CA} \sin^4\theta_F \sin 4(\delta_F - \beta) \right] = 0, \quad (7)$$

$$\frac{\partial F}{\partial \theta_F} = m_S \left\{ H_{ext}[\sin\theta_H \cos\theta_F \cos(\delta_F - \delta_H) - \cos\theta_H \sin\theta_F] \right.$$
$$+ 2\pi m_S \left(1 - \frac{H_{OA}}{4\pi m_S} \right) \sin 2\theta_F + \frac{1}{2} H_{SA} \cos^2\delta_F \sin 2\theta_F$$
$$\left. - \frac{1}{4} H_{CA} \left[\sin 4\theta_F + 2\sin^3\theta_F \sin^2 2(\delta_F - \beta) \right] \right\} = 0. \quad (8)$$

f_R can thus be determined from[23]

$$f_R = \frac{\gamma}{2\pi} \frac{1}{m_S} \sqrt{\frac{\partial^2 F}{\partial \theta_F^2} \frac{\partial^2 F}{\partial \delta_F^2} - \left(\frac{\partial^2 F}{\partial \theta_F \partial \delta_F} \right)^2}. \quad (9)$$

The f_R–H_{ext} relation at $\theta_H = 45°$ are well reproduced by the numerical simulation based on Eq. (9), as shown in Fig. 2(f). In the simulation, $m_S = 808$ emu/cm^3 is characterized from DC magnetometry. $\mu_0 H_{OA} = 0.35$ T, $\mu_0 H_{SA} = 18$ mT, $\mu_0 H_{CA} = 17$ mT, and

$\beta = 55°$ are determined from best fit. The small effective demagnetization field ($4\pi\mu_0 m_S - \mu_0 H_{OA} = 0.65$ T) is also possibly attributed to the finite junction size and the effect of dipolar field.[24] It is noted that the experimental results show higher f_R around the minimum ($\mu_0 H = -50$ mT or 10 mT). This can be explained by the higher H_{effm} contributed by the edge effects and defects, resulting in higher f_R according to Eq. (3). The validity of this model is further confirmed by the similar φ-H_{ext} relation between the simulation (Fig. 2(f), inset) and the calculation based on experiment (Fig. 2(b)).

In order to further investigate the influence of the tilt angle of the hard-plane magnetic field, f_R is plotted as a function of θ_H in Fig. 3(a). The measured f_R exhibits a minimum at $\theta_H = 10°$–$15°$, and then gradually increases at larger θ_H. To reveal the mechanism behind this angular dependence, the equilibrium angles (θ_F, δ_F) of **m** under the hard-plane magnetic field ($\mu_0 H_{ext} = -0.1$ T) tilted by different θ_H are calculated based on Eqs. (7) and (8) and shown in the right axis of Fig. 3(b). The f_R–θ_H relation is qualitatively interpreted by Eq. (3). At small θ_H, the IP effective field is dominated by IP anisotropy. As θ_H increases from 0° to 10°–15°, H_{effm} gradually decreases as the increasing IP component of H_{ext} overshadows the anisotropy. Meanwhile, **m** rotates away towards the y-axis ($-\delta_F$ increasing from $<40°$ to 102° in the right axis of Fig. 3(b)), resulting in declining H_{effm} and thus decreasing f_R. When $\theta_H > 15°$, **m** is maintained near the y-axis. As θ_H increases, the angle between H_{ext} and **m** decreases from 60° to ~0°. The H_{effm} increases as the effect of H_{ext} on **m** increases, leading to increasing f_R with θ_H. The numerical simulation based on Eq. (9) exhibits similar trend as compared to the experimental result at $\mu_0 H_{ext} = -0.1$ T (Fig. 3(b), left axis). The difference in f_R between the experiments and simulations when $\theta_H < 10°$ is believed to be resulted from the loss of single domain state under weak IP effective field. Further, the f_R and V_{DC} at different H_{ext} and θ_H are shown in Figs. 3(c) and 3(d), respectively, to evaluate the influence of magnitude and direction of magnetic field. f_R is higher under larger H_{ext} and larger θ_H. The minimum f_R in
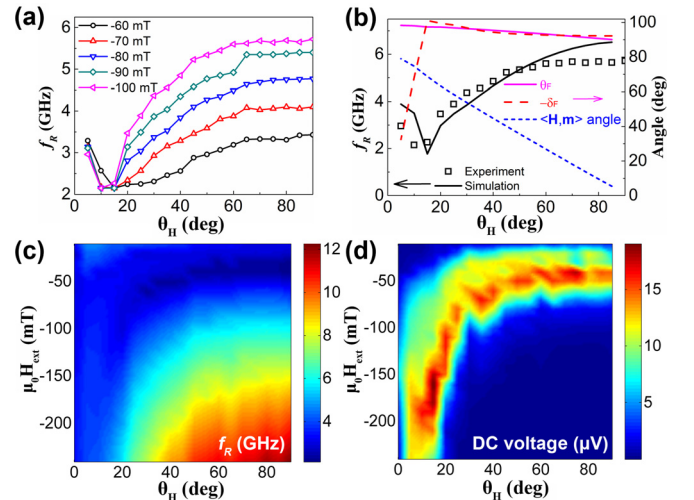

FIG. 3. Influence of θ_H when $\delta_H = 90°$ (a) f_R as a function of θ_H. (b) Calculated θ_F, δ_F and angle between H_{ext} and **m** (right y-axis) and measured (square) and simulated (solid line) f_R (left y-axis) as a function of θ_H with $\mu_0 H_{ext} = -100$ mT. (c) f_R and (d) V_{DC} as a function of H_{ext} and θ_H.

Fig. 3(c) coincides with the maximum V_{DC} in Fig. 3(d). This can be interpreted by the maximum φ when **m** is parallel to the hard axis. It is noted that at smaller θ_H, V_{DC} reaches maximum under larger H_{ext}. When $\theta_H = 15°$, the largest V_{DC} of $19.9\,\mu V$ is achieved at $-160\,mT$. While at $\theta_H = 60°$, V_{DC} reaches maximum of $16.3\,\mu V$ at $-40\,mT$. This is because when θ_H is smaller, larger H_{ext} is required to provide sufficient IP component ($H_{ext}sin\theta_H$) to saturate the free layer. These results indicate that both the magnitude and the OOP angle of magnetic field are effective in tuning the f_R and V_{DC}.

Finally, in order to evaluate how the performance of the spin torque diode detector can be tuned by the OOP angle of the magnetic field, the sensitivity and f_R at $\theta_H = 0°$–$90°$ and $\delta_H = 30°$–$90°$ are characterized. V_{DC} and f_R at $\mu_0 H_{ext} = -0.1\,T$ are shown in Figs. 4(a) and 4(b), respectively. Higher V_{DC} is achieved at larger δ_H. This is because V_{mix} is proportional to $sin^2\varphi$ (Eq. (2)), and larger φ is expected when the magnetic field is applied towards the hard axis (large δ_H). V_{DC} reaches maximum at $\theta_H = 20°$ and $\delta_H = 90°$, accompanied with the minimum f_R. This can be explained by the smaller H_{effm} when larger φ exists. As interpreted in Fig. 3(d), θ_H corresponding to the maximum V_{DC} gradually decreases with increasing H_{ext}. f_R is relatively higher when θ_H approaches $90°$. This is consistent with the observation that f_R increases with θ_H in Fig. 3(a). The maximum sensitivity (Fig. 4(c)) and the frequency bandwidth (Fig. 4(d)) are defined as the highest sensitivity and the frequency range between the maximum and minimum f_R, respectively, when $\mu_0 H_{ext}$ is changed from $-0.01\,T$ to $-0.2\,T$.

Similar to Fig. 4(a), high sensitivity is achieved at large δ_H. The bandwidth is primarily determined by f_R at $\mu_0 H_{ext} = -0.2\,T$, so Fig. 4(d) exhibits similar angular dependence with Fig. 4(b). The 3 dB field range and f_R range are shown, respectively, in Figs. 4(e) and 4(f) to illustrate the range of H_{ext} and f_R where the sensitivity is higher than 50% ($-3\,dB$) of the maximum at a certain field angle. The 3 dB field range is larger at small θ_H, due to the smaller V_{dc}–H_{ext} dependence when the magnetic field rotates towards OOP, as shown in Fig. 2(d). However, the larger 3 dB field range when θ_H approaches $0°$ only results in small 3 dB f_R range. This can be illustrated by the low field dependence of f_R at small θ_H, as shown in Fig. 2(e). Through combined analysis of the maximum sensitivity, bandwidth, and 3 dB f_R range, the performance of the microwave detector over the full field range can be evaluated. The optimized maximum sensitivity of 19.9 mV/ mW (or 151 mV/mW after correction of impedance mismatch) is observed at $\theta_H = 15°$ and $\delta_H = 90°$. This indicates 29% increase in sensitivity compared with the case of IP magnetic field (15.7 mV/mW at $\theta_H = 90°$ and $\delta_H = 90°$). The bandwidth of 1.1 GHz and 3 dB f_R range of 1 GHz indicates that high sensitivity is granted in most of the frequency band. On the other hand, widest bandwidth of 9.8 GHz is achieved when $\theta_H = 90°$ and $\delta_H = 30°$, and this bandwidth is expected to be further extended when δ_F is smaller than $30°$. However, the corresponding low maximum sensitivity (0.11 mV/mW) and 3 dB f_R range (2.24 GHz) indicate poor microwave detectivity. Although the co-existence of wide 3 dB f_R range and high sensitivity remains to be difficult, a compromised performance can be achieved by fine-tuning the tilt angle of the magnetic field. For example, the direction of the magnetic field can be set to be $\theta_H = 30°$ and $\delta_H = 90°$ to achieve a bandwidth of 4.49 GHz and maximum sensitivity of 14.7 mV/mW (or 103 mV/mW after correction). The 3 dB f_R range of 2.21 GHz indicates high sensitivity can be achieved at half of the frequency band. Or one can achieve high sensitivity of 17.3 mV/ mW (or 121 mV/mW after correction) and 3 dB f_R range of 1.6 GHz at $\theta_H = 75°$ and $\delta_H = 90°$. The wide bandwidth of 7.5 GHz offers some perspective for application in extended frequency band with moderate sensitivity. The sensitivity is expected to be further increased through improving the TMR ratio, reducing junction resistance for impedance matching, applying DC bias current,[25] and exploiting materials with low saturation magnetization as free layer.

In summary, this work demonstrates that the bandwidth and sensitivity of spin-torque microwave detectors can be optimized through changing the direction of magnetic field. The influence of the angle and magnitude of hard-plane magnetic field on the f_R and V_{DC} is investigated. The V-shape reliance of f_R on H_{ext} and on θ_H is qualitatively explicated by Kittel's ferromagnetic resonance model and quantitatively reproduced by an analytical model. Maximum V_{DC} is observed at minimum f_R due to the largest φ at that point. The performance of the spin-torque diode detector is evaluated under three-dimensional magnetic field. Frequency bandwidth up to 9.8 GHz or sensitivity up to 19.9 mV/mW (or 151 mV/mW after correction) can be achieved by applying magnetic field with different OOP angles. The sensitivity and frequency bandwidth can be flexibly tailored based on
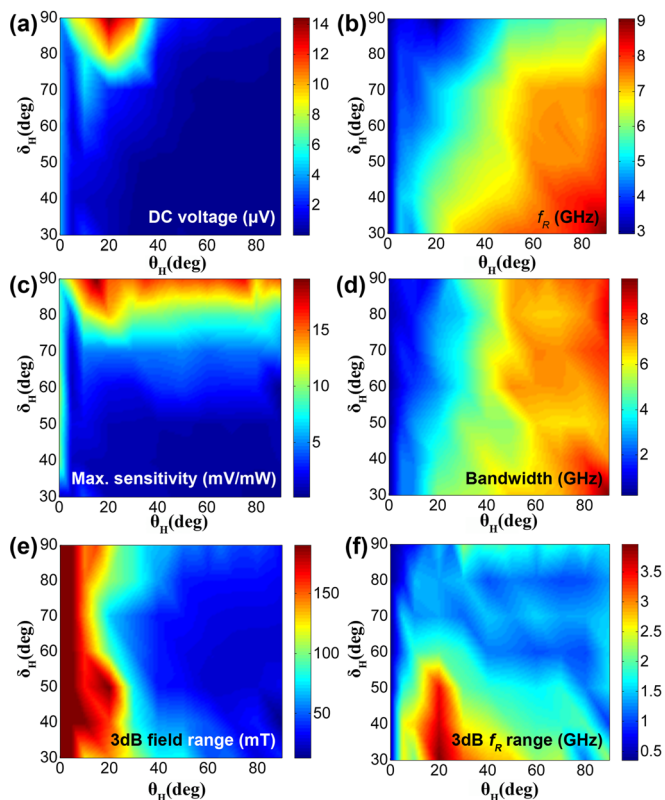

FIG. 4. Influence of the OOP angle of the magnetic field: (a) V_{DC} and (b) f_R under $\mu_0 H_{ext} = -0.1\,T$ and (c) the maximum sensitivity, (d) the frequency bandwidth, (e) the 3 dB field range, and (f) the 3 dB f_R range when $\mu_0 H_{ext}$ is swept from -0.01 to $-0.2\,T$.

the specific requirements through tuning the OOP angle of the magnetic field.

[1]S. I. Kiselev, J. C. Sankey, I. N. Krivorotov, N. C. Emley, R. J. Schoelkopf, R. A. Buhrman, and D. C. Ralph, Nature **425**, 380 (2003).

[2]A. A. Tulapurkar, Y. Suzuki, A. Fukushima, H. Kubota, H. Maehara, K. Tsunekawa, D. D. Djayaprawira, N. Watanabe, and S. Yuasa, Nature **438**, 339 (2005).

[3]S. Hemour, Y. Zhao, C. H. P. Lorenz, D. Houssameddine, Y. Gui, C.-M. Hu, and K. Wu, IEEE Trans. Microwave Theory Tech. **62**, 965 (2014).

[4]X. Fan, R. Cao, T. Moriyama, W. Wang, H. W. Zhang, and J. Q. Xiao, Appl. Phys. Lett. **95**, 122501 (2009).

[5]S. Miwa, S. Ishibashi, H. Tomita, T. Nozaki, E. Tamura, K. Ando, N. Mizuochi, T. Saruya, H. Kubota, K. Yakushiji, T. Taniguchi, H. Imamura, A. Fukushima, S. Yuasa, and Y. Suzuki, Nat. Mater. **13**, 50 (2014).

[6]B. Fang, M. Carpentieri, X. Hao, H. Jiang, J. A. Katine, I. N. Krivorotov, B. Ocker, J. Langer, K. L. Wang, B. Zhang, B. Azzerboni, P. K. Amiri, G. Finocchio, and Z. Zeng, Nat. Commun. **7**, 11259 (2016).

[7]C. Wang, Y.-T. Cui, J. Z. Sun, J. A. Katine, R. A. Buhrman, and D. C. Ralph, J. Appl. Phys. **106**, 053905 (2009).

[8]T. Taniguchi and H. Imamura, Appl. Phys. Express **6**, 053002 (2013).

[9]D. Bang, T. Taniguchi, H. Kubota, T. Yorozu, H. Imamura, K. Yakushiji, A. Fukushima, S. Yuasa, and K. Ando, J. Appl. Phys. **111**, 07C917 (2012).

[10]T. Taniguchi and H. Imamura, J. Appl. Phys. **114**, 053903 (2013).

[11]X. Cheng, J. A. Katine, G. E. Rowlands, and I. N. Krivorotov, Appl. Phys. Lett. **103**, 082402 (2013).

[12]C. Wang, Y. T. Cui, J. Z. Sun, J. A. Katine, R. A. Buhrman, and D. C. Ralph, Phys. Rev. B **79**, 224416 (2009).

[13]W. X. Wang, Y. Yang, H. Naganuma, Y. Ando, R. C. Yu, and X. F. Han, Appl. Phys. Lett. **99**, 012502 (2011).

[14]S. Ikeda, K. Miura, H. Yamamoto, K. Mizunuma, H. D. Gan, M. Endo, S. Kanai, J. Hayakawa, F. Matsukura, and H. Ohno, Nat. Mater. **9**, 721 (2010).

[15]S. Yakata, H. Kubota, Y. Suzuki, K. Yakushiji, A. Fukushima, S. Yuasa, and K. Ando, J. Appl. Phys. **105**, 07D131 (2009).

[16]R. Matsumoto, A. Chanthbouala, J. Grollier, V. Cros, A. Fert, K. Nishimura, Y. Nagamine, H. Maehara, K. Tsunekawa, A. Fukushima, and S. Yuasa, Appl. Phys. Express **4**, 063001 (2011).

[17]S. Yuasa, Y. Suzuki, T. Katayama, and K. Ando, Appl. Phys. Lett. **87**, 242503 (2005).

[18]C. Kittel, Phys. Rev. **71**, 270 (1947).

[19]C. Kittel, Phys. Rev. **73**, 155 (1948).

[20]Z. Zeng, K. H. Cheung, H. W. Jiang, I. N. Krivorotov, J. A. Katine, V. Tiberkevich, and A. Slavin, Phys. Rev. B **82**, 100410 (2010).

[21]R. Matsumoto, H. Kubota, T. Yamaji, H. Arai, S. Yuasa, and H. Imamura, Jpn. J. Appl. Phys. **53**, 123001 (2014).

[22]Y. V. Goryunov, N. N. Garifyanov, G. G. Khaliullin, I. A. Garifullin, L. R. Tagirov, F. Schreiber, T. Muhge, and H. Zabel, Phys. Rev. B **52**, 13450 (1995).

[23]H. Suhl, Phys. Rev. **97**, 555 (1955).

[24]W. Chen, G. de Loubens, J.-M. L. Beaujour, A. D. Kent, and J. Z. Sun, J. Appl. Phys. **103**, 07A502 (2008).

[25]S. Ishibashi, K. Ando, T. Seki, T. Nozaki, H. Kubota, S. Yakata, H. Maehara, A. Fukushima, S. Yuasa, and Y. Suzuki, IEEE Trans. Magn. **47**, 3373 (2011).